



Adsorption of drinking water fluoride on a micron-sized magnetic Fe₃O₄@Fe-Ti composite adsorbent



Chang Zhang, Yingzhen Li, Ting-Jie Wang*, Yanping Jiang, Haifeng Wang

Department of Chemical Engineering, Tsinghua University, 100084 Beijing, China

ARTICLE INFO

Article history:

Received 3 October 2015
Received in revised form 7 December 2015
Accepted 9 December 2015
Available online 13 December 2015

Keywords:

Fluoride
Adsorbent
Regeneration
Co-existing ion
Drinking water

ABSTRACT

A micron-sized magnetic adsorbent (MMA) for fluoride removal from drinking water was prepared by spray drying and subsequent calcination of a magnetic Fe₃O₄@Fe-Ti core-shell nanoparticle slurry. The MMA granules had high mechanical strength and stability against water scouring, can be easily separated from the water by a magnet, and had a high selectivity for fluoride versus common co-existing ions and high fluoride removal efficiency in a wide range of initial pH of 3–11. Abundant hydroxyl groups on the MMA surface acted as the active sites for fluoride adsorption, which resulted in a high affinity of the MMA for fluoride. The pH in the adsorption process affected the adsorption significantly. At neutral initial pH, the adsorption isotherm was well fitted with the Langmuir model, and the maximum adsorption capacity reached a high value of 41.8 mg/g. At a constant pH of 3, multilayer adsorption of fluoride occurred due to the abundant positive surface charges on the MMA, and the adsorption isotherm was well fitted with the Freundlich model. The MMA had a fast adsorption rate, and adsorption equilibrium was achieved within 2 min. The adsorption kinetics followed a quasi-second order model. The regeneration of the MMA was easy and fast, and can be completed within 2 min. After 10 recycles, the fluoride removal efficiency of the MMA still remained high. These properties showed that the MMA is a promising adsorbent for fluoride removal.

© 2015 Elsevier B.V. All rights reserved.

1. Introduction

Excessive fluoride ingestion is very harmful to human health. Drinking water is the main source of human fluoride intake; so the defluoridation of drinking water with excess fluoride is necessary for human health [1–3]. The most widely used defluoridation method is adsorption because of its high removal efficiency, low cost and easy operation [3]. Many kinds of nanoscaled metal oxides have been considered for defluoridation adsorbents in recent years, because they have high adsorption rates and capacities compared to traditional adsorbents [4,5]. Among these adsorbents, iron-based multi-metallic oxides such as Fe(III)-Al(III) [6], Fe(III)-Zr(IV) [7], Fe(III)-Cr(III) [8], Fe(III)-Sn(IV) [9], and Fe(III)-Ti(IV) [10–12] have attracted more attention for their high adsorption capacity and low cost.

However, due to their tiny size, nano-sized metal oxide adsorbents are hard to separate from water, and the nanoparticle residues cause secondary pollution and safety problems for the drinking water. Researchers have combined nano-adsorbents with

magnetic core particles by surface coating and other methods to enhance adsorbent particle separation from water by magnetic assistance [5,12–20] to get a higher separation efficiency and lessen the residues in the water. However, the effective and complete separation of the nanoparticles from the water is still difficult. Compared to nanoparticles, micron or larger sized particles with magnetism can be separated from water more efficiently in industry [21–24]. Therefore, a promising method is to granulate the nano-adsorbents into a larger size for the safe and efficient practical defluoridation of drinking water. Millimeter or larger sized granulation needs binders to increase the strength of the granules. However, binders would adsorb on active sites and cause a significant loss of adsorption capacity. In addition, the large size of the granules would easily result in diffusion limitation of the adsorption process and desorption in the subsequent regeneration [3,25–28]. Therefore, micron sized granulation is desirable because it can both meet the requirement of separation efficiency and avoid the loss of adsorption capacity and adsorption rate.

The initial pH and co-existing ions have a significant influence on the performance of the adsorbent in fluoride removal. Most adsorbents have a narrow pH range available for fluoride removal, and their adsorption capacities decrease significantly beyond the suitable pH range, resulting in their limited practical application.

* Corresponding author.

E-mail address: wangtj@tsinghua.edu.cn (T.-J. Wang).

Moreover, the influences of the initial pH on adsorption capacity are affected by the structure and surface properties of the adsorbent [4,28–32]. Therefore, how the surface structure of the adsorbent affect the pH range and the adsorption mechanism need to be studied. In nature, there are a lot of co-existing ions with fluoride in groundwater, e.g., the concentration of F^- is usually less than 4 mg/L in groundwater, while the concentration of Cl^- and SO_4^{2-} in groundwater can reach several hundred mg per liter [33]. However, in most cases studied in the literature, the concentrations of the co-existing ions were less than 100 mg/L along with a relatively high fluoride concentration [5,13,15,28,29], which did not represent well the selectivity the adsorbent would have with actual groundwater. Even in this case, the adsorption capacity of the metal oxide adsorbent still decreased significantly with the co-existence of other ions, especially HCO_3^- , SO_4^{2-} and PO_4^{3-} . For example, the adsorption capacity of crystalline titanium showed a 30% loss in the presence of HCO_3^- at 61 mg/L [4], the adsorption capacity of bismuth oxides (HBOs) decreased by 40% in the presence of 96 mg/L SO_4^{2-} [30], a Fe-Al-Ce adsorbent exhibited only 40% of the initial adsorption capacity in the presence of only 3 mg/L PO_4^{3-} [31], etc. The competition by co-existing ions is a significant limitation of fluoride removal. Therefore, a fluoride adsorbent with a high affinity to fluoride versus other ions is highly desirable.

Adsorbent regeneration is an important part in the defluoridation of drinking water, which affects the efficiency and cost of fluoride removal. However, the regeneration for many metal oxide adsorbents is a time consuming and inefficient process, and the adsorption capacity after regeneration can decrease significantly. For example, the desorption efficiency of crystalline titanium was only 79%, and the adsorption capacity decreased to 50% after regeneration [4]. The decrease of adsorption capacity after the regeneration for schwertmannite was as high as 78% [28]. An aluminum-alginate composite adsorbent had an optimized desorption efficiency of merely 69%, and the regeneration process required 20 h [32]. Inefficient regeneration leads to poor reusability of the adsorbent and high cost. Therefore, an adsorbent that can be easily regenerated for long-term recycling is significant for effective fluoride removal.

In this paper, a novel micron-sized magnetic adsorbent (MMA) was prepared by granulating a $Fe_3O_4@Fe-Ti$ core-shell composite to achieve a safe and effective defluoridation process for drinking water. The mechanic stability against water scouring and magnetic separation efficiency of the MMA were studied. The fluoride removal efficiency of the MMA at different pH and different co-existing ions was investigated. The surface structure and adsorption mechanism as well as the adsorption isotherm and kinetics of the MMA were discussed. The regeneration efficiency of the adsorbent was examined to verify the reusability of the MMA.

2. Materials and experiments

2.1. Material

$FeCl_3 \cdot 6H_2O$ (Sinopharm Chemical Reagent Company, China), $FeCl_2 \cdot 4H_2O$ (Shantou Xilong Chemical Co., Ltd., China), $FeSO_4 \cdot 7H_2O$ (Beijing Chemical Plant, China), $Ti(SO_4)_2 \cdot 12H_2O$ (Sinopharm Chemical Reagent Company, China), HCl acid (Beijing Chemical Plant, China), NaOH, cetyltrimethyl ammonium bromide (CTAB, Tianjin Bodi Chemical Co., Ltd., China), NaF (Beijing Modern East Fine Chemicals Co., Ltd., China), ammonia (Beijing Modern East Fine Chemicals Co., Ltd., China), and anhydrous ethanol (Beijing Modern East Fine Chemicals Co., Ltd., China) were used in the preparation and characterization of the MMA granules. NaCl, $NaNO_3$, Na_2SO_4 , Na_2SiO_3 , Na_2CO_3 , Na_3PO_4 , $CaCl_2$ and $MgCl_2$ were used to form the

co-existing ions in the fluoride bearing water. All the chemicals were analytical grade and were used without further purification.

2.2. Preparation of the MMA granules

The preparation of the MMA granules has two steps: first, the preparation of the magnetic $Fe_3O_4@Fe-Ti$ core-shell nanoparticles, i.e., the Fe-Ti shell materials coated on the surface of the Fe_3O_4 core particle, which was described in our previous work [12], and second, the granulation of the $Fe_3O_4@Fe-Ti$ nanoparticles. The preparation of the magnetic $Fe_3O_4@Fe-Ti$ nanoparticles was as follows. (1) Preparation of superparamagnetic Fe_3O_4 nanoparticles: $FeCl_2 \cdot 4H_2O$ and $FeCl_3 \cdot 6H_2O$ were dissolved in ethanol at a molar ratio of 5:1, then the mixed solution was slowly titrated using ammonia under agitation until the pH reached 9.0. The nanoparticles of Fe_3O_4 were selected using a magnet, and then re-dispersed in deionized water for further use. (2) Coating of the Fe-Ti bimetallic oxide onto the surface of the Fe_3O_4 nanoparticle: Equal molar amounts of $FeSO_4 \cdot 7H_2O$ and $Ti(SO_4)_2$ were dissolved in deionized water, forming a mixed solution. The solution was slowly titrated into the prepared Fe_3O_4 nanoparticle suspension, which was adjusted to $pH = 4 \pm 0.2$ using ammonia solution during the titration process. Then the magnetic $Fe_3O_4@Fe-Ti$ nanoparticles were collected using a magnet.

The granulation of the $Fe_3O_4@Fe-Ti$ nanoparticles was performed as follows: the $Fe_3O_4@Fe-Ti$ nanoparticles were washed 3 times with deionized water. Afterwards, the suspension of the washed nanoparticles at 0.1 g/mL was pumped into an experiment-scaled spray dryer (YC 015, Shanghai Pilotech Instrument & Equipment Co., Ltd., China) at a rate of 20 mL/min. The inner diameter of the nozzle was 1.5 mm. The inlet air temperature was set at 200 °C. The outlet temperature of the gas was 80 °C. The micron-sized granules were collected and heated at 200 °C for 1.5 h in a muffle furnace; thus, the MMA granules were obtained.

2.3. Characterization

The microstructure and morphology of the MMA granules were examined by a scanning electron microscopy (SEM, Carl ZeissMerlin, Germany). The size distribution was measured by a Malvern laser analyzer (Mastersizer 3000, Malvern, UK). The pore volume and specific surface area of MMA were measured by nitrogen adsorption with an Autosorb-iQ2-C (Quantachrome Instruments, USA). The magnetism of the adsorbent was analyzed by a vibrating sample magnetometer (VSM, 7307, Lake shore, USA). The chemical structure of the adsorbent before and after defluoridation was examined by Fourier transform infrared spectroscopy (FT-IR, Thermo Nicolet 560, USA) and X-ray photoelectron spectroscopy (XPS, PHI Quantera SXM, ULVAC-PHI, Japan). The surface potential of the adsorbent at different pH was measured using a zeta potential instrument (ZetaPALS, Brookhaven Instruments Corporation, USA).

2.4. Adsorption performance

The adsorption performance of the MMA granules was examined by batch experiments. 100 mg adsorbent was added to 100 mL fluoride solution (the adsorbent dosage remained unchanged unless specially stated), and the sample vessel was shaken on a thermostat shaker at 180 rpm and 25 °C for 1 h (the shaking conditions were kept unchanged unless specially stated). The fluoride concentration at equilibrium was measured by a fluoride ion meter (PXS-450, Shanghai Kangyi Instrument Co., Ltd., China) and a fluoride electrode (PF1, Shanghai Kangyi Instrument Co., Ltd., China), from which the adsorption capacity and fluoride removal efficiency were calculated. The equilibrium adsorption capacity (Q_e , mg/g) was defined as the mass ratio of adsorbed fluoride to the adsorbent.

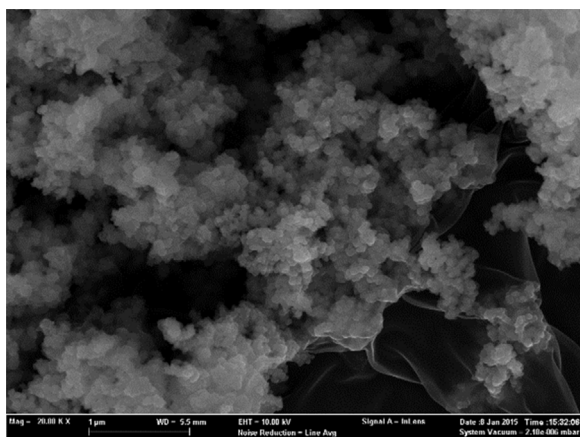


Fig. 1. SEM image of the MMA.

The fluoride removal efficiency (R , %) was defined as the percentage of adsorbed fluoride of the initial fluoride concentration. The pH value of the solution was monitored by an experiment-scaled pH meter (FiveEasy/FE20, Mettler Toledo, Switzerland).

The Fe residue in water after magnetic separation was measured by polarized Zeeman atomic adsorption spectroscopy (AAS, Z-5000, Hitachi High-Technologies Corp., Japan).

2.5. Effects of pH and co-existing ions

To investigate the effects of pH on adsorption, the initial pH of the fluoride solution was adjusted for a range of 2–12 using HCl or NaOH solution. The initial fluoride concentration was set at 4 mg/L. The pH and adsorption capacity were measured at equilibrium.

To investigate the effects of co-existing ions on adsorption, NaCl, NaNO₃, Na₂SO₄, Na₂SiO₃, Na₂CO₃, Na₃PO₄, CaCl₂, MgCl₂ were added into the fluoride solution to provide Cl⁻, NO₃⁻, SO₄²⁻, SiO₃²⁻, HCO₃⁻, PO₄³⁻, Ca²⁺, Mg²⁺, respectively. The molar ratio of the co-existing ions to fluoride was set to be 1:1, 10:1 and 100:1. The initial pH was adjusted to 7–8 using HCl or NaOH solution. The initial fluoride concentration was set at 4 mg/L. The pH and adsorption capacity were measured at equilibrium.

2.6. Regeneration

After the adsorption reached equilibrium in a fluoride solution, the MMA granules were collected and re-dispersed in NaOH solution at a set concentration under shaking to desorb the fluoride from the surface of the adsorbent. After a set time, the fluoride concentration in the solution was measured, and the regeneration efficiency, namely, the percentage of desorbed fluoride relative to the total adsorbed fluoride was calculated. The desorption percentage for desorption process at various NaOH concentrations was measured to get the desorption rate and saturated regeneration efficiency.

After desorption by NaOH solution for a set time, the MMA granules were collected and washed with HCl solution at the same concentration as that of NaOH, then re-collected and dispersed in a fluoride solution for next recycle adsorption. This was a regeneration cycle. To evaluate the reusability of MMA, the adsorption efficiency of MMA in 10 regeneration cycles was measured.

3. Results and discussion

3.1. Properties of the MMA granules

The SEM images of the MMA granules in Fig. 1 showed that the MMA granules were agglomerates of nanoparticles with a

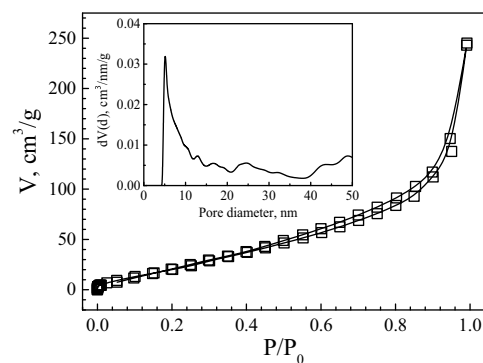


Fig. 2. N₂ adsorption–desorption isotherm of the MMA. Inset: pore size distribution analyzed by DFT method.

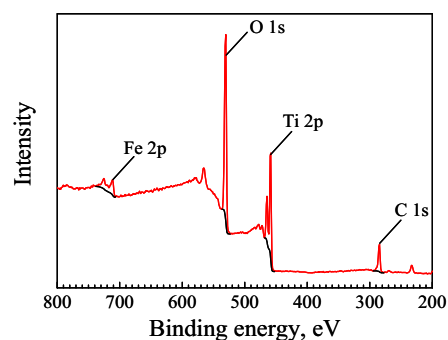


Fig. 3. XPS spectra of the MMA.

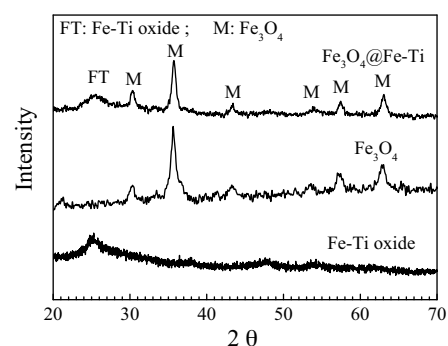


Fig. 4. XRD spectra of the MMA, Fe₃O₄ and Fe-Ti oxide.

primary size of about 20 nm. The microstructure of the MMA indicated a high porosity and a large surface area. The N₂ adsorption–desorption isotherm was measured, as shown in Fig. 2, and analyzed using ASiQwin V2.0 software. The inset of pore size distribution in Fig. 2 showed a peak at 5.2 nm, and all the pores were larger than 4.5 nm. These meso and macro pores were formed due to the aggregation of nanoparticles, which was consistent with the SEM observation. The total pore volume of the MMA granules was calculated to be 0.38 cm³/g, and the specific surface area (analyzed by the BET equation) of the MMA granules was calculated to be 99.2 m²/g. The high pore volume and specific surface area of the MMA granules indicated a high capacity potential for fluoride adsorption.

The XPS spectra of the MMA is shown in Fig. 3. The characteristic peaks at 711.6 eV, 530.7 eV and 459.0 eV were assigned to Fe2p, O1s and Ti2p, respectively, indicating the Fe, O and Ti component in MMA. The XRD pattern of the MMA is shown in Fig. 4. It is clearly shown that the XRD spectrum of the Fe₃O₄@Fe-Ti MMA was a combination of Fe₃O₄ and Fe-Ti oxide. The characteristic peaks at 30.3°,

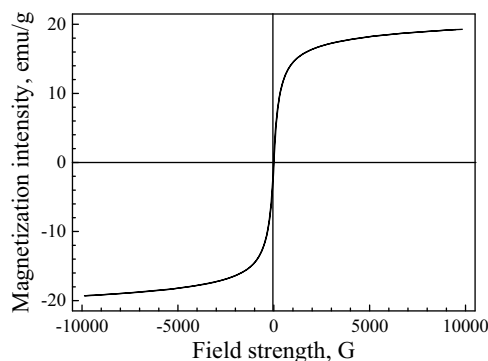


Fig. 5. Magnetic properties of the MMA.

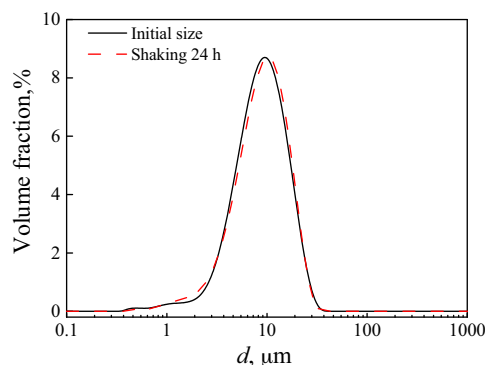


Fig. 6. Size distribution of the MMA before and after shaking for 24 h.

35.6°, 43.2°, 53.8°, 57.5°, 63.2° were assigned to crystalline magnetite (Fe_3O_4), while the broad peak at 25.3° was attributed to the amorphous Fe-Ti oxide.

The hysteresis loop of the MMA granules shown in Fig. 5 illustrated that the MMA granules had superparamagnetism. The saturation magnetization was 19.3 emu/g, which was a high magnetic strength compared to those in related literature reports [5,12–15]. This indicated that the MMA granules can be separated effectively from water using a magnet. The average size of the MMA granules was determined as 10.1 μm by a Malvern laser analyzer, as shown in Fig. 6, which is suitable for magnetic separation [21–24].

In order to verify the stability of the MMA granules, 50 mg MMA granules was put in a conical flask filled with 50 mL water, and the flask was shaken on a thermostat shaker at 180 rpm and 25 °C for 24 h. The size distribution of the MMA granules after shaking was measured and compared with that before shaking. These are shown in Fig. 6. The size distribution of the MMA granules before and after shaking changed very little, indicating a high stability against water scouring. This indicated that the MMA granules can meet the demand of granule stability for an adsorbent for the fluoride removing process for drinking water.

To verify the separability of the MMA granules, a $50 \times 50 \times 10 \text{ mm}^3$ Nd-Fe-B magnet (N30, 1.08–1.12 T) was used for the separation of the MMA granules from water. It was observed that the MMA granules moved quickly to the magnet and the water became clear soon. After 5 min, the concentration of total Fe in the supernatant was reduced to 0.12 mg/L, which is lower than the upper limit of 0.30 mg/L set by the safety standard of China (GB5749-2006) for drinking water. The data showed that the MMA granules had high stability against water scouring and can be separated efficiently from water by a magnet; thus, they can be used for water treatment.

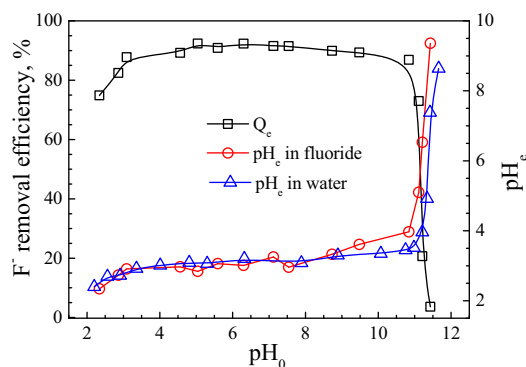


Fig. 7. Effects of pH on the fluoride removal efficiency of MMA (initial $[\text{F}^-] = 4 \text{ mg/L}$).

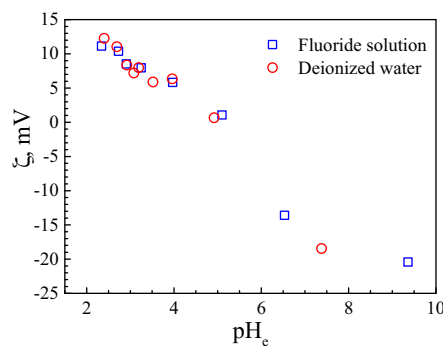


Fig. 8. Effects of pH on the zeta potential of MMA in water/fluoride.

3.2. Effects of the initial pH on adsorption performance

The changes in fluoride removal efficiency and equilibrium pH value versus the initial pH of the fluoride solution are shown in Fig. 7. For the initial $[\text{F}^-]$ of 4 mg/L and 1 g/L adsorbent dosage of the MMA, the fluoride removal efficiency reached 86.9%–92.4% at the initial pH range of 3–11, indicating that the MMA can be used in a wide pH range of fluoride solution, which was much wider than those in related reports [4,24–28]. This indicated that the MMA had a high affinity for fluoride ions. When the initial pH was lower than 3, the formation of HF was enhanced, leading to the decrease of the adsorption efficiency. When the initial pH was higher than 11, the equilibrium pH increased sharply. Accordingly, the surface zeta potential of the MMA granules decreased as shown in Fig. 8, and the electrostatic interaction between the MMA surface and F^- was weakened. In addition, the competition by OH^- versus fluoride ions also led to the decrease of removal efficiency at a high initial pH of the fluoride solution.

Fig. 7 showed that the MMA has a strong buffering effect for the solution pH at the initial pH range of 3–11. The equilibrium pH in both water and fluoride solutions was near 3. This was due to the interaction of the MMA surface with the H^+ and OH^- in the solution. When the initial pH was higher than 8, the equilibrium pH in the fluoride solution was a little higher than that in water, which may be due to the competition of fluoride ions and OH^- .

The buffering effect of the MMA was due to the hydroxylation of the metal oxide in water [34]. The metal ions on the surface layer of the metal oxide have unsaturated coordination; thus, they served as a Lewis acid (electron acceptor) [34] to coordinate water molecules:



The surface groups reacted with H^+ and OH^- by



Table 1
Effects of different co-existing anions on fluoride removal efficiency of MMA.

Mole ratio to [F ⁻]	1:1		10:1		100:1	
	F ⁻ removal, %	pH _e	F ⁻ removal, %	pH _e	F ⁻ removal, %	pH _e
–	90.6	2.94	90.6	2.94	90.6	2.94
Cl ⁻	92.6	3.31	92.3	3.25	90.6	2.80
NO ₃ ⁻	91.0	2.95	91.4	2.87	89.5	2.84
SO ₄ ²⁻	92.0	3.27	89.3	3.33	90.5	3.21
SiO ₃ ²⁻	91.7	3.16	87.2	3.15	64.4	4.81
HCO ₃ ⁻	93.9	3.35	76.3	4.82	7.7	7.46
PO ₄ ³⁻	90.9	3.20	31.1	5.50	7.7	6.67



These reactions balanced the concentrations of OH⁻ and H⁺ in water, and kept the pH value stabilized near 3. When OH⁻ was at a high concentration, the reactions of Eqs. (3) and (4) were enhanced; then OH⁻ was consumed and the pH decreased. When H⁺ was at a high concentration, the reverse reaction of Eq. (2) was enhanced and the pH increased. These resulted in a buffering effect on the solution pH. When the amounts of OH⁻ and H⁺ bonded on the MMA surface were changed, the surface charges changed accordingly as shown in Fig. 8, which also confirmed the above reactions.

The wide buffering range indicated a high density of hydroxyl groups on the surface of the MMA. It was inferred that the acidic equilibrium pH was due to the high affinity of ≡MOH₂⁺ and ≡MOH for OH⁻. When the surface was positively charged, the surface hydroxyl groups only existed as ≡MOH₂⁺ and ≡MOH. The amounts of hydroxyl groups ≡MOH₂⁺ and ≡MOH can be measured by excess acid/alkali reactions of the MMA. The measurement was conducted as follows: 50 mg MMA was added into 50 mL HCl solution. The pH of the HCl solution was chosen to be beyond the range of the MMA's buffering effect to ensure the acid was in excess. In Fig. 4, a HCl solution of pH=2 was chosen for the excess acid reaction. ≡MOH groups on the surface of the MMA react with H⁺ in the solution by the reverse reaction of Eq. (2), and ≡MOH₂⁺ does not consume H⁺. Therefore, the consumption of H⁺ was equal to the total amount of ≡MOH on the surface of the MMA; therefore,

$$\{\equiv\text{MOH}\} = \Delta[\text{H}^+] \quad (5)$$

When the titration reached equilibrium, the consumption of [H⁺] was determined to be 1.64 mM/g, i.e., [≡MOH] = 1.64 mM/g.

In the case of alkali reaction, a NaOH solution of pH = 12 was chosen, and 50 mg MMA was added into 50 mL NaOH solution. ≡MOH₂⁺ and ≡MOH react with OH⁻ as in Eqs. (3) and (4), and all of the ≡MOH₂⁺ and ≡MOH are involved in the reactions. After one ≡MOH₂⁺ reacted with one OH⁻, the product ≡MOH can still consume one OH⁻; thus one ≡MOH₂⁺ can consume two OH⁻, and one ≡MOH can consume one OH⁻; so,

$$\Delta[\text{OH}^-] = 2 \times \{\equiv\text{MOH}_2^+\} + \{\equiv\text{MOH}\} \quad (6)$$

From Eqs. (5) and (6), the amount of ≡MOH₂⁺ was

$$\{\equiv\text{MOH}_2^+\} = 0.5 \times (\Delta[\text{OH}^-] - \Delta[\text{H}^+]) \quad (7)$$

Since the surface hydroxyl groups only existed as ≡MOH₂⁺ and ≡MOH, the total amount of hydroxyl groups was

$$\{\equiv\text{M}\}_t = \{\equiv\text{MOH}_2^+\} + \{\equiv\text{MOH}\} \quad (8)$$

When the titration reached equilibrium, the consumption of [OH⁻] was determined to be 3.54 mM/g. From Eqs. (7) and (8), it was calculated that {MOH₂⁺} = 0.95 mM/g, {M}_t = 2.59 mM/g. With the specific surface area of the MMA as 99.2 m²/g, the average density of hydroxyl on the MMA surface was 15.7 OH/nm², which was much higher than that of typical oxides, which are 4–10 OH/nm² [35].

The addition of the MMA would turn neutral water into acidic water at pH = 3; so, some alkali such as NaOH is needed to neutralize the acidic water. It was calculated that 1 L water needed only 1 mM NaOH. This only caused a 23 mg/L increase of Na⁺, which is negligible, compared to the common concentration of Na⁺ (>200 mg/L). There is no upper limit for Na⁺ in the safety standard for drinking water of China (GB5749-2006).

3.3. Effects of co-existing ions on adsorption performance

Fluoride bearing groundwater usually contains many co-existing ions. A high selectivity of the adsorbent for fluoride is essential for achieving high fluoride removal efficiency. The effects of common co-existing ions, including Cl⁻, NO₃⁻, SO₄²⁻, SiO₃²⁻, HCO₃⁻, PO₄³⁻, Ca²⁺, Mg²⁺, on fluoride removal efficiency were investigated at the concentrations of 1, 10 and 100 times (i.e., 0.21 mM, 2.1 mM, 21 mM) the fluoride mole concentration. The initial pH of the fluoride bearing water was adjusted to 7–8 in these experiments.

The fluoride removal efficiency of the MMA in the presence of the different co-existing anions in the fluoride solution is listed in Table 1. Cl⁻, NO₃⁻, SO₄²⁻ had little effect on the fluoride removal efficiency even at 100 times the fluoride molar concentration (i.e., 747 mg/L, 1305 mg/L, 2021 mg/L for Cl⁻, NO₃⁻, SO₄²⁻, respectively). The data also showed that the ion strength has no effect on the fluoride removal efficiency, which confirmed the formation of a tight inner-sphere complex on the surface of the MMA [14,15].

SiO₃²⁻, HCO₃⁻ and PO₄³⁻ at high concentrations affected the fluoride removal efficiency of MMA, as shown in Table 1. It was inferred that these anions compete with F⁻ for the adsorption sites because they are also chemically bonded on the surface of the MMA to form inner-sphere complexes [4,14,28,36]. Even so, the MMA still had a high selectivity against these anions at a relatively high concentration. The fluoride removal efficiency of MMA basically remained unaffected until the concentrations of SiO₃²⁻ and PO₄³⁻ reached 160 mg/L and 20 mg/L, respectively. The fluoride removal efficiency of MMA only had a small decrease of 15.7% when the HCO₃⁻ concentration was at 126 mg/L. These data indicated that the MMA has excellent selectivity to fluoride compared to the adsorbents reported in the literature [4,5,13,27,31,37,38].

In the presence of Cl⁻, NO₃⁻ and SO₄²⁻, the equilibrium pH of the solution remained the same as in the blank experiment. In the presence of SiO₃²⁻, HCO₃⁻ and PO₄³⁻, the equilibrium pH of the solution showed a significant increase, and a higher equilibrium pH corresponded lower adsorption capacity. This indicated that the increase of the equilibrium pH caused by the addition of SiO₃²⁻, HCO₃⁻ and PO₄³⁻ might also have contributed to the decrease of fluoride removal efficiency.

Considering the similarity between chloride and fluoride, the effects of a wider range of chloride concentration on the fluoride removal efficiency were investigated, as shown in Table 2. It is observed that in the range of 0–1000 mM/L, Cl⁻ had no obvious effects on fluoride removal efficiency. This also confirmed the

Table 2
Effects of Cl⁻ concentration on the fluoride removal efficiency of MMA.

C(Cl ⁻), mM	0	0.1	1	10	100	1000
F ⁻ removal, %	91.5	90.3	90.9	91.8	91.6	90.0
pH _e	3.25	3.16	3.14	3.07	3.04	2.96

Table 3
Effects of Ca²⁺ and Mg²⁺ on fluoride removal efficiency of MMA.

Cation	C, mg/L	F ⁻ removal, %	pH _e
Ca ²⁺	866.8	89.2	3.34
Mg ²⁺	511.9	87.1	3.40
-	-	90.6	3.25

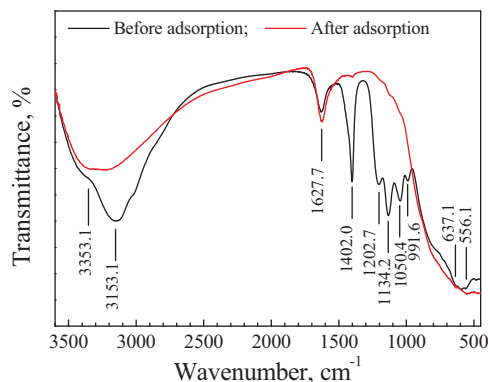


Fig. 9. FT-IR spectra of MMA before and after adsorption (Initial [F⁻] = 200 mg/L).

formation of an inner-sphere complex in the fluoride adsorption process.

The effects of Ca²⁺ and Mg²⁺ on fluoride removal efficiency are shown in Table 3. When the mole concentrations of Ca²⁺ and Mg²⁺ were 100 times that of the fluoride, i.e., 866.8 mg/L and 511.9 mg/L for Ca²⁺ and Mg²⁺, respectively, the fluoride removal efficiency was almost unaffected, showing that the MMA is feasible for use for fluoride removal from magnesium-rich and calcium-rich groundwater.

Therefore, it was verified that the MMA has a high selectivity for fluoride and can be used in practical water treatment environments with various initial pH values and co-existing ions.

3.4. Adsorption mechanism of the MMA

The high adsorption selectivity and capacity of the MMA for fluoride were due to the surface structure of the MMA. The FT-IR spectra of the MMA before and after fluoride adsorption are shown in Fig. 9. In the spectrum before adsorption, the characteristics of the hydroxyl group were obvious. The bands at 3353.1 cm⁻¹ and 1627.7 cm⁻¹ were assigned to the stretching and bending vibrations of water [11]; the band at 3153.1 cm⁻¹ was assigned to the stretching vibration of hydroxyl [39,40]; the band at 1402.0 cm⁻¹ may be associated with gaseous water [41]; and the bands at 1202.7 cm⁻¹, 1134.2 cm⁻¹, 1050.4 cm⁻¹, 991.6 cm⁻¹ were assigned to the bending vibration of hydroxyl [11]. The bands at 637.1 cm⁻¹ and 556.1 cm⁻¹ were the characteristic bands of Ti-O and Fe-O, respectively [11,41,42]. After adsorption, the band at 3153.1 cm⁻¹ was weakened, and the bands at 1202.7 cm⁻¹, 1134.2 cm⁻¹, 1050.4 cm⁻¹, 991.6 cm⁻¹ disappeared, indicating the surface hydroxyl of MMA played a significant role in fluoride adsorption.

The O1s XPS spectra of MMA before and after adsorption are shown in Fig. 10. The O1s spectra was deconvoluted into two peaks. The one at 532.0 eV was assigned to the hydroxyl (OH) and the other at 530.4 eV was assigned to the oxygen anion (O²⁻). It is observed

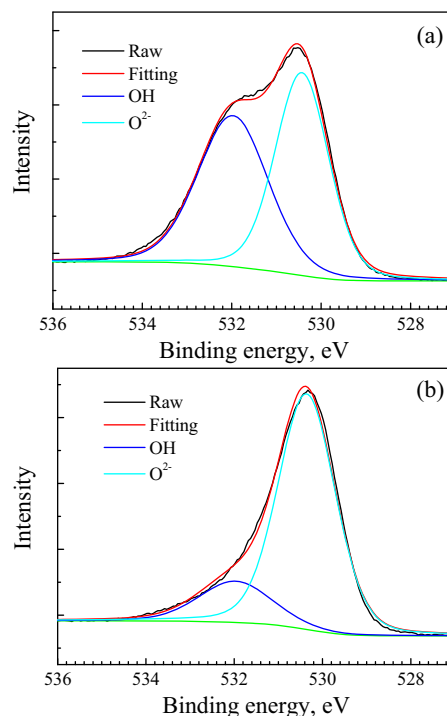


Fig. 10. XPS spectra of MMA (a) before and (b) after adsorption (Initial [F⁻] = 200 mg/L).

Table 4
Changes of the XPS O1s peak of MMA before and after adsorption (Initial [F⁻] = 200 mg/L).

Sample	Peak	Binding energy, eV	FWHM, eV	Mole content, %
MMA	O ²⁻	530.4	1.41	58.1
	OH ⁻	532.0	1.85	56.7
MMA-F	O ²⁻	530.4	1.53	82.5
	OH ⁻	532.0	1.95	18.4

that the OH peak decreased after adsorption. The percentages of OH and O²⁻ before and after adsorption are listed in Table 4. The fraction of OH decreased from 56.7% to 18.4% after adsorption, while the fraction of O²⁻ increased from 58.1% to 82.5%. Meanwhile, the F 1s peak at 684.3 eV appeared in the XPS spectra after adsorption, confirming that fluoride was adsorbed on the surface of the MMA. This peak was not found before adsorption. These data suggested that surface hydroxyl groups were replaced by fluoride [43,44].

Therefore, it is inferred that the reactions that occurred on the MMA surface in the adsorption process were



where M represents the surface metal species. As discussed in our previous work [11], there is a synergistic interaction between Fe and Ti in the Fe-Ti oxide for fluoride adsorption, resulting in the much higher adsorption capacity of Fe-Ti oxide than that of the pure iron oxide and titanium oxide prepared in the same process. The positive shift of Ti2p from pure Ti oxide to Fe-Ti oxide in XPS spectra confirmed the formation of Fe-O-Ti bond. A further positive shift of Ti2p in Fe-Ti oxide after fluoride adsorption confirmed the formation of Fe-O-Ti-F bond. Therefore, M in Eqs. (9) and (10) is Fe-O-Ti, representing the active site for fluoride adsorption.

According to Eq. (10), fluoride adsorption caused OH⁻ release; thus the pH of the solution would increase with the increase of the fluoride concentration. To verify this, the equilibrium pH of the

Table 5
Equilibrium pH and zeta potential at different initial $[F^-]_0$ with uncontrolled/constant pH.

$[F^-]_0$, mg/L	0	4	37.5	50	100	150	200
pH _e	3.08	3.25	3.91	4.23	4.81	4.91	5.36
ζ (pH ₀ = 7, pH uncontrolled), mV	7.20	7.95	-3.5	-4.9	-15.1	-17.0	-18.0
ζ (controlled pH = 3), mV	8.86	7.95	5.2	3.3	-5.3	-6.3	-7.2

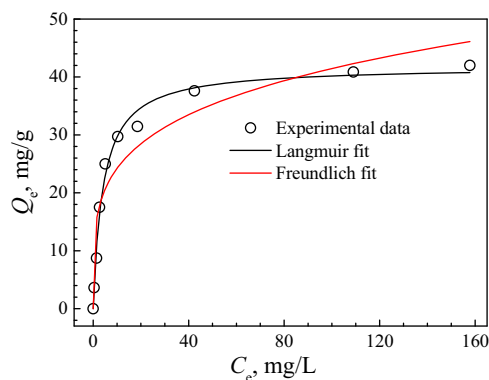


Fig. 11. Adsorption isotherms on MMA at unadjusted pH (adsorbent dosage = 1 g/L).

fluoride removal systems at different fluoride concentrations with neutral initial pH and no adjustment during adsorption were measured, and listed in Table 5. When the initial $[F^-]$ increased from 4 mg/L to 200 mg/L, the equilibrium pH increased from 3.3 to 5.4, which confirmed the reaction of Eq. (10).

3.5. Adsorption isotherms of the MMA

The Langmuir model and Freundlich model are usually used to describe adsorption behavior [3]. In Langmuir model,

$$Q_e = \frac{Q_{L,max} b C_e}{1 + b C_e} \quad (11)$$

where $Q_{L,max}$ is the maximum monolayer adsorption capacity, and b represents the binding affinity [10,12]. The Langmuir model assumes the adsorption to be a homogeneous process.

In Freundlich model,

$$Q_e = K_f C_e^{1/n} \quad (12)$$

where K_f and n represent the adsorption capacity and binding energy, respectively [4,10]. The Freundlich model describes a heterogeneous and multi-layer adsorption process.

The fluoride adsorption isotherm of MMA without control of the pH was measured, and shown in Fig. 11. The fluoride solutions had a neutral initial pH, and there was no pH control in the adsorption process. The adsorption isotherm data were fitted using the Langmuir model and Freundlich model. The fitting results are listed in Table 6. Fig. 11 and Table 6 show that the adsorption isotherm was better fitted with the Langmuir model than the Freundlich model. The maximum adsorption capacity of MMA reached a high value of 41.8 mg/g.

However, as shown in Table 5, the equilibrium pH of these systems increased with the increase of initial fluoride concentration due to the ion exchange of fluoride and hydroxyl. This resulted in a change of the active sites on the MMA surface. Therefore, the solution pH in the adsorption process was adjusted using HCl solution to keep the $pH = 3 \pm 0.2$, which equals the equilibrium pH of the MMA in a pure water system. This ensured that the surface hydroxyl sites of the MMA were kept the same as the fluoride-free condition in the adsorption process for the different initial fluoride concentrations. Under this condition, the adsorption isotherm was measured and fitted with the Langmuir model and Freundlich

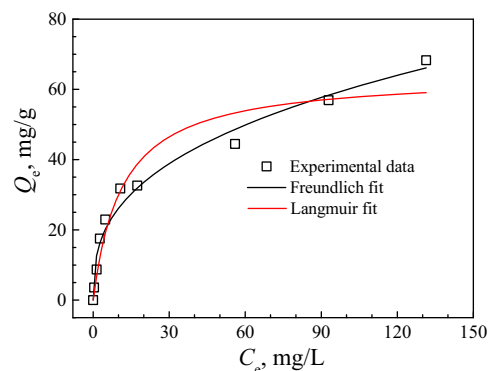


Fig. 12. Adsorption isotherms at constant pH (adsorbent dosage = 1 g/L).

model, as shown in Fig. 12. The fitting parameters are listed in Table 6. The adsorption isotherm data at constant pH were better fitted with the Freundlich model than Langmuir model. The equilibrium adsorption capacity at the initial fluoride of 200 mg/L was 68.3 mg/g, that is, 3.59 mM/g, while the surface hydroxyl density obtained from the excess acid/alkali reactions was only 2.59 mM/g. This indicated the occurrence of multilayer adsorption, which fitted the Freundlich model.

Different surface hydroxyl states result in different surface charges. As shown in Table 5, at constant pH = 3, the surface charges of the MMA at adsorption equilibrium were significantly higher than those with no control of the pH. This was because the added H^+ in the condition of constant pH = 3 balanced the OH^- released during the adsorption process, or adsorbed on the surface of the MMA, thus enhancing the fluoride adsorption. After the first adsorption layer on the surface of the MMA was saturated, the adsorption process continued and multilayer adsorption occurred, fitting the Freundlich model. However, for the solution with neutral initial pH and no pH control in the adsorption process, the surface positive charges were less; thus the adsorption process did not go on after the saturation of first adsorption layer, namely, monolayer adsorption occurred, fitting the Langmuir model.

The adsorption capacity of the MMA at neutral initial pH was compared with similar samples in previous literatures, as shown in Table 7. It is shown that the MMA had a relatively high saturated adsorption capacity and also a high equilibrium adsorption capacity at $[F^-]_0 = 10$ mg/L compared with similar samples, ensuring an effective adsorption in actual groundwater environment, for the fluoride level in groundwater is mostly less than 10 mg/L. In addition, the preparation of the MMA are facile and cost-effective. No noble metal was needed, and no toxic ions leached like Al. Therefore, the MMA granules are very competitive in practical application.

3.6. Adsorption kinetics and regeneration of the MMA

The adsorption capacity of the MMA changed with time as shown in Fig. 13. The initial fluoride solution was at a concentration of 4 mg/L and at neutral pH, and the solution pH was not controlled in the adsorption process. The adsorption rate data were well fitted with a quasi-second order kinetic model with a

Table 6
Fitting parameters of the adsorption isotherms of MMA.

Parameter	Langmuir isotherm model			Freundlich isotherm model		
	$Q_{L,max}$, mg/g	b , L/mg	R^2	K_f , mg/g	n	R^2
pH ₀ = 7, pH uncontrolled	41.83	0.24	0.9902	14.16	4.29	0.8988
Controlled pH = 3	64.21	0.09	0.9388	11.40	2.77	0.9768

Table 7
Comparison of adsorption capacities of the MMA granules and similar samples in previous literatures.

Sample	$Q_{L,max}$, mg/g	Q_e at $[F^-]_0 = 10$ mg/L	Initial pH	References
Crystalline TiO ₂	0.3	0.3	7.3	[4]
Sulfate-doped Fe ₃ O ₄ /Al ₂ O ₃	70.4	9.2	7	[5]
Fe-Al mixed oxide	17.7	9.1	6.9	[6]
Fe-Zr mixed oxide	6.9	5.1	6.8	[7]
Fe-Cr mixed oxide	16	7.1	6.5	[8]
Fe-Sn mixed oxide	10.5	2.9	6.4	[9]
Fe ₃ O ₄ @Al(OH) ₃	88.5	9.5	6.5	[13]
Al(OH) ₃ /SiO ₂ /Fe ₃ O ₄	38	2.6	6	[14]
ZrO ₂ /SiO ₂ /Fe ₃ O ₄	14.7	6.3	4	[15]
Fe ₃ O ₄ /APTES/Zr	–	0.9	5.5	[16]
Mg-Al-LDH	40.2	6.7	5	[27]
Schwertmannite(Fe ₈ O ₈ (OH) ₆ SO ₄)	55.3	7.6	–	[28]
Nano-sized goethite (α-FeOOH)	59.0	6.0	6–8	[29]
Hydrous bismuth oxides (HBOs)	1.9	0.3	7	[30]
Fe-Al-Ce trimetal oxide	195.0	9.2	7	[31]
Aluminum alginate	76.4	5.3	1.5	[32]
Basic aluminum sulfate@graphene hydrogel composites	68.9	8.3	7.2	[37]
Ultrasound assisted Mg-Al-LDH	47.7	7.7	5.5	[38]
Fe ₃ O ₄ @Fe-Ti oxide	41.8	8.7	7	This work

Table 8
Fluoride adsorption efficiency of MMA for 10 regeneration recycles.

Recycles	1	2	3	4	5	6	7	8	9	10
F ⁻ removal, %	87.3	87.4	88.2	85.8	86.5	81.0	86.1	80.9	81.5	77.0

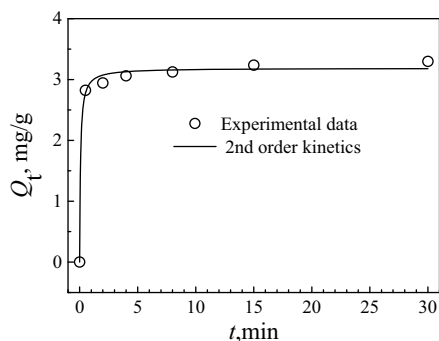


Fig. 13. Adsorption kinetics of MMA (initial $[F^-] = 4$ mg/L, adsorbent dosage = 1 g/L, uncontrolled pH).

correlation coefficient of 0.9938, and the rate constant was 4.24 g/mg/min. The adsorption was fast and reached equilibrium within 2 min.

Fast and effective regeneration of an adsorbent is highly desirable. Fig. 14 shows the regeneration efficiency, namely, the desorption percentages of fluoride, during the desorption process using 0.001 M, 0.005 M and 0.01 M NaOH solution. The regeneration was quite fast and reached equilibrium within 2 min. The regeneration efficiency increased with increasing concentration of the NaOH solution, and reached 91.4%, 96.2% and 96.8% with 0.001 M, 0.005 M and 0.01 M, respectively. Therefore, it is shown that the MMA can be effectively regenerated with NaOH solution.

To illustrate the reusability of the MMA for fluoride removal, the fluoride removal efficiency of the MMA in 10 regeneration recycles is shown in Table 8. The regeneration was conducted

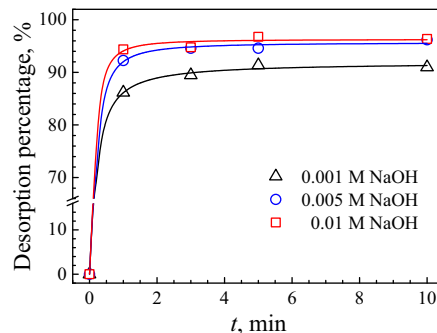


Fig. 14. Regeneration with different concentrations of the NaOH solution.

using 0.01 M NaOH solution. The adsorption efficiency showed little decrease after 5 recycles, while it decreased slightly by 11.8% after 10 recycles. That is still sufficient for fluoride removal utility. This suggested that the MMA can be reused in a long-term process and still has high adsorption efficiency.

4. Conclusion

A novel micron-sized magnetic adsorbent (MMA) for the defluoridation of drinking water was prepared by spray drying and calcination of magnetic Fe₃O₄@Fe-Ti core-shell nanoparticles prepared by chemical precipitation and surface coating. These MMA granules have good stability and high magnetic strength for easy separation from water with a magnet. The granules have a high fluoride removal efficiency in a wide range of pH = 3–11, and a high selectivity for fluoride versus common ions. Abundant hydroxyl

groups on the surface of the MMA acted as the active sites for fluoride adsorption. The pH in the adsorption process affected the adsorption performance significantly. At neutral initial pH, the adsorption isotherm was well fitted with the Langmuir model with a maximum adsorption capacity of 41.8 mg/g. At a constant pH of 3, the MMA surface had a high affinity for fluoride, which gave multi-layer adsorption, which was well fitted with the Freundlich model. The adsorption kinetics was well fitted with a quasi-second order model. Adsorption equilibrium was achieved within 2 min. The regeneration of the MMA using NaOH solution was easy and fast, and reached equilibrium within 2 min. The adsorption efficiency remained high after 10 regeneration cycles. These properties indicated that the MMA is promising for fluoride removal.

Acknowledgements

The authors wish to express their appreciation of financial support of this study by National High Technology Research and Development Program (863 Program, No. 2012AA062605) and the National Natural Science Foundation of China (NSFC, No. 21176134).

References

- [1] M. Mohapatra, S. Anand, B.K. Mishra, D.E. Giles, P. Singh, Review of fluoride removal from drinking water, *J. Environ. Manag.* 91 (2009) 67–77.
- [2] S. Meenakshi, R.C. Maheshwari, Fluoride in drinking water and its removal, *J. Hazard. Mater.* 137 (2006) 456–463.
- [3] A. Bhatnagar, E. Kumar, M. Sillanpää, Fluoride removal from water by adsorption—A review, *Chem. Eng. J.* 171 (2011) 811–840.
- [4] K. Babaeivini, A.P. Khodadoust, Adsorption of fluoride onto crystalline titanium dioxide: effect of pH, ionic strength, and co-existing ions, *J. Coll. Interf. Sci.* 394 (2013) 419–427.
- [5] L. Chai, Y. Wang, N. Zhao, W. Yang, X. You, Sulfate-doped Fe₃O₄/Al₂O₃ nanoparticles as a novel adsorbent for fluoride removal from drinking water, *Water Res.* 47 (2013) 4040–4049.
- [6] K. Biswas, S.K. Saha, U.C. Ghosh, Adsorption of fluoride from aqueous solution by a synthetic iron(III)-aluminum(III) mixed oxide, *Ind. Eng. Chem. Res.* 46 (2007) 5346–5356.
- [7] K. Biswas, D. Bandhoyadhyay, U.C. Ghosh, Adsorption kinetics of fluoride on iron(III)-zirconium(IV) hybrid oxide, *Adsorption* 13 (2007) 83–94.
- [8] K. Biswas, S. Debnath, U.C. Ghosh, Physicochemical aspects on fluoride adsorption for removal from water by synthetic hydrous iron(III)-chromium(III) mixed oxide, *Sep. Sci. Technol.* 45 (2010) 472–485.
- [9] K. Biswas, K. Gupta, U.C. Ghosh, Adsorption of fluoride by hydrous iron(III)-tin(IV) bimetal mixed oxide from the aqueous solutions, *Chem. Eng. J.* 149 (2009) 196–206.
- [10] L. Chen, S. He, B.Y. He, T.J. Wang, C.L. Su, C. Zhang, Y. Jin, Synthesis of iron-doped titanium oxide nano-adsorbent and its adsorption characteristics for fluoride in drinking water, *Ind. Eng. Chem. Res.* 51 (2012) 13150–13156.
- [11] L. Chen, B.Y. He, S. He, T.J. Wang, C.L. Su, Y. Jin, Fe-Ti oxide nano-adsorbent synthesized by co-precipitation for fluoride removal from drinking water and its adsorption mechanism, *Powder Technol.* 227 (2012) 3–8.
- [12] C. Zhang, L. Chen, T.J. Wang, C.L. Su, Y. Jin, Synthesis and properties of a magnetic core-shell composite nano-adsorbent for fluoride removal from drinking water, *Appl. Surf. Sci.* 317 (2014) 552–559.
- [13] X. Zhao, J. Wang, F. Wu, T. Wang, Y. Cai, Y. Shi, G. Jiang, Removal of fluoride from aqueous media by Fe₃O₄@Al(OH)₃ magnetic nano-particles, *J. Hazard. Mater.* 173 (2010) 102–109.
- [14] C.-F. Chang, P.-H. Lin, W. Höll, Aluminum-type superparamagnetic adsorbents: Synthesis and application on fluoride removal, *Coll. Surf. A: Physicochem. Eng. Asp.* 280 (2006) 194–202.
- [15] C.-F. Chang, C.Y. Chang, T.L. Hsu, Removal of fluoride from aqueous solution with the superparamagnetic zirconia material, *Desalination* 279 (2011) 375–382.
- [16] T. Poursaberi, M. Hassanisadi, K. Torkestani, M. Zare, Development of zirconium (IV)-metalloporphyrin grafted Fe₃O₄ nano-particles for efficient fluoride removal, *Chem. Eng. J.* 189–190 (2012) 117–125.
- [17] M. Stefana, C. Leosteană, O. Panaa, M.-L. Sorana, R.C. Suciua, E. Gautronb, O. Chauvet, Synthesis and characterization of Fe₃O₄@ZnS and Fe₃O₄@Au@ZnS core-shell nanoparticles, *Appl. Surf. Sci.* 288 (2014) 180–192.
- [18] X.B. Fang, Z.Q. Fang, P.K.E. Tsang, W. Cheng, X.M. Yan, L.C. Zheng, Selective adsorption of Cr(VI) from aqueous solution by EDA-Fe₃O₄ nanoparticles prepared from steel pickling waste liquor, *Appl. Surf. Sci.* 314 (2014) 655–662.
- [19] J. Ma, S. Guo, X. Guo, H. Ge, A mild synthetic route to Fe₃O₄@TiO₂-Au composites: preparation, characterization and photocatalytic activity, *Appl. Surf. Sci.* 353 (2015) 1117–1125.
- [20] K. Ouyang, C. Zhu, Y. Zhao, L. Wang, S. Xie, Q. Wang, Adsorption mechanism of magnetically separable Fe₃O₄/graphene oxide hybrids, *Appl. Surf. Sci.* 355 (2015) 562–569.
- [21] R.D. Ambashta, M. Sillanpää, Water purification using magnetic assistance: a review, *J. Hazard. Mater.* 180 (2010) 38–49.
- [22] A. Funes, J. de Vicente, L. Cruz-Pizarro, I. de Vicente, The influence of pH on manganese removal by magnetic microparticles in solution, *Water Res.* 53 (2014) 110–122.
- [23] R. Gerber, R.R. Birss, High gradient magnetic separation, *Research Studies Press*, 1983.
- [24] T. Dong, Q. Su, Z. Yang, Y. Zhang, E.B. Egeland, D.D. Gu, A smart fully integrated micromachined separator with soft magnetic micro-pillar arrays for cell isolation, *J. Micromech. Microeng.* 20 (2010) 115–121.
- [25] M. Habuda-Stanić, M. Ravančić, A. Flanagan, A review on adsorption of fluoride from aqueous solution, *Materials* 7 (2014) 6317–6366.
- [26] M. Badruzzaman, P. Westerhoff, D.R. Knappe, Intraparticle diffusion and adsorption of arsenate onto granular ferric hydroxide (GFH), *Water Res.* 38 (2004) 4002–4012.
- [27] C. Gao, X.Y. Yu, T. Luo, Y. Jia, B. Sun, J.H. Liu, Millimeter-sized Mg-Al-LDH nanoflake impregnated magnetic alginate beads (LDH-n-MABs): a novel bio-based sorbent for the removal of fluoride in water, *J. Mater. Chem. A* 2 (2014) 2119–2128.
- [28] A. Eskandarpour, M.S. Onyango, A. Ochieng, S. Asai, Removal of fluoride ions from aqueous solution at low pH using schwertmannite, *J. Hazard. Mater.* 152 (2008) 571–579.
- [29] M. Mohapatra, K. Rout, S.K. Gupta, P. Singh, S. Anand, B.K. Mishra, Facile synthesis of additive-assisted nano goethite powder and its application for fluoride remediation, *J. Nanopart. Res.* 12 (2009) 681–686.
- [30] A.L. Srivastav, P.K. Singh, V. Srivastava, Y.C. Sharma, Application of a new adsorbent for fluoride removal from aqueous solutions, *J. Hazard. Mater.* 263 (2013) 342–352.
- [31] X. Wu, Y. Zhang, X. Dou, M. Yang, Fluoride removal performance of a novel Fe-Al-Ce trimetal oxide adsorbent, *Chemosphere* 69 (2007) 1758–1764.
- [32] Q. Zhou, X. Lin, B. Li, X. Luo, Fluoride adsorption from aqueous solution by aluminum alginate particles prepared via electrostatic spinning device, *Chem. Eng. J.* 256 (2014) 306–315.
- [33] C. Li, Z. Wei, Groundwater Quality and Pollution, China Architecture & Building Press, Beijing, 1983.
- [34] N. Anderson, A.J. Rubin, Adsorption of Inorganics at Solid-liquid Interfaces, Ann Arbor Science Publishers Inc., 1981.
- [35] C.-P. Huang, W. Stumm, Specific adsorption of cations on hydrous γ-Al₂O₃, *J. Coll. Interf. Sci.* 43 (1973) 409–420.
- [36] A. Zach-Maor, R. Semiat, H. Shemer, Fixed bed phosphate adsorption by immobilized nano-magnetite matrix: experimental and a new modeling approach, *Adsorption* 17 (2011) 929–936.
- [37] Y.Q. Chen, Q.K. Zhang, L.B. Chen, H. Bai, L. Li, Basic aluminum sulfate/graphene hydrogel composites: preparation and application for removal of fluoride, *J. Mater. Chem. A* 1 (2013) 13101–13110.
- [38] Q. Chang, L. Zhu, Z. Luo, M. Lei, S. Zhang, H. Tang, Sono-assisted preparation of magnetic magnesium-aluminum layered double hydroxides and their application for removing fluoride, *Ultrason. Sonochem.* 18 (2011) 553–561.
- [39] J. Russell, R. Parfitt, A. Fraser, V. Farmer, Surface structures of gibbsite goethite and phosphated goethite, *Nature* 248 (1974) 220–221.
- [40] R.J. Atkinson, R.L. Parfitt, R.S.C. Smart, Infra-red study of phosphate adsorption on goethite, *J. Chem. Soc. Faraday Trans.* 70 (1974) 1472–1479.
- [41] M.N. Kopylovich, A.M. Kirillov, A.K. Baev, A.J.L. Pombeiro, Heteronuclear iron(III)-chromium(III) hydroxo complexes and hydroxides, and their catalytic activity towards peroxidative oxidation of alkanes, *J. Mol. Catal. A: Chemical* 206 (2003) 163–178.
- [42] N. Papassiopi, K. Vaxevanidou, C. Christou, E. Karagianni, G.S. Antipas, Synthesis, characterization and stability of Cr(III) and Fe(III) hydroxides, *J. Hazard. Mater.* 264 (2014) 490–497.
- [43] C. Minero, G. Mariella, V. Maurino, E. Pelizzetti, Photocatalytic transformation of organic compounds in the presence of inorganic anions. 1. Hydroxyl-mediated and direct electron-transfer reactions of phenol on a titanium dioxide-fluoride system, *Langmuir* 16 (2000) 2632–2641.
- [44] K. Lv, B. Cheng, J. Yu, G. Liu, Fluorine ions-mediated morphology control of anatase TiO₂ with enhanced photocatalytic activity, *Phys. Chem. Chem. Phys.* 14 (2012) 5349–5362.